JOURNAL OF APPLIED ELECTROCHEMISTRY **20** (1990) 912–915

The wall-jet electrode and the study of electrode reaction mechanisms: the EC reaction

R. G. COMPTON, A. C. FISHER, G. P. TYLEY

Physical Chemistry Laboratory, Oxford University, South Parks Road, OXFORD OX1 3QZ, UK

Received 29 January 1990; revised 22 March 1990

The theory of EC reactions at a wall-jet electrode is developed using a computational procedure based on the Backwards Implicit Method. In particular, for the case of a reversible electron transfer, it is shown that the variation of the halfwave potential with solution flow rate provides a means of characterizing the EC mechanism. A working curve is presented which permits the analysis of experimental data and the deduction of the rate constant for the following chemical reaction.

Nomenclature

a	diameter of the jet
a_j	matrix element ($j = 2, 3, \ldots, \overline{J-1}$)
b_j	matrix element ($j = 1, 2, \ldots, \overline{J-1}$)
C_j	matrix element ($j = 1, 2, \ldots, \overline{J-1}$)
D	diffusion coefficient
$\mathbf{d}_j$	vector element ($j = 1, 2, \ldots, \overline{J-1}$)
E	electrode potential
E^0	standard electrode potential of A/B couple
F	Faraday constant
$g(\mathrm{A})$	normalized concentration of A
$g(\mathrm{B})$	normalized concentration of B
I	current
I_{LIM}	transport limited current
J	number of points in r-direction on finite difference grid
j	counter, $j = 1, 2, \ldots, J$
K	Number of points in z-direction on finite difference grid
$K_{j,k+1}$	normalized rate constant (Equation 23)
k	counter, $k = 1, 2, \ldots, K$
k'	counter, $k' = 1, 2, \ldots, K$
k_c	experimental constant
$\tilde{k}$	first order rate constant
M	constant defined by $M = k_c^4 V_f^3 / 2\pi^3 a^2$
R	electrode radius
r	radial coordinate
$\mathbf{u}_j$	vector element ($j = 1, 2, \ldots, \overline{J-1}$)
V	volume flow rate ($\mathrm{cm^3\,s^{-1}}$)
v_r	solution velocity in r-direction
v_z	solution velocity in z-direction
z	coordinate normal to electrode surface
η	dimensionless distance parameter (see Equation 5)
ξ	dimensionless variable (Equation 25)
θ	normalized electrode potential
$\theta_{1/2}$	normalized halfwave potential
ν	kinematic viscosity ($\mathrm{cm^2\,s^{-1}}$)
χ	dimensionless variable (Equation 26)
$\{\mathbf{d}\}_k$	vector $\{d_{1,k}, d_{2,k}, \ldots, d_{J-1,k}\}$
$\{\mathbf{u}\}_k$	vector $\{u_{1,k+1}, u_{2,k+1}, \ldots, u_{J-1,k+1}\}$

1. Introduction

The wall-jet electrode (WJE) is a well-defined hydrodynamic electrode in which the flow is due to a jet of fluid which impinges normally onto a planar electrode surface and spreads out radially over that surface, the fluid outside the jet being at rest [1]. Whilst the WJE has found considerable application in electroanalysis [2–12] its application in the study of electrode reaction mechanisms, particularly those involving coupled homogeneous kinetics, is limited. In part this is because of the lack of appropriate theory for the interpretation of such experiments [13]. Accordingly in an earlier paper [13] we developed a general computational method for solving mass transport problems involving wall-jet electrodes and, in particular, developed the theory for the transport limited current/flow behaviour for simple electron transfer reactions, and for ECE and DISPI processes. In the former case satisfactory agreement with existing analytical approaches was noted [14, 15], and in the latter case our computations were shown to be in good agreement with experiment [16].

In our previous calculations [13, 16] we used the backwards implicit finite difference (BIFD) method to calculate transport limited currents as a function of solution flow rate and electrode geometry. In this paper we show how to extend these calculations to the computation of the shape of current/voltage curves and, in particular, consider the EC mechanism,

$$\mathrm{A} + e^- \rightleftharpoons \mathrm{B} \qquad \text{(i)}$$

$$\mathrm{B} \xrightarrow{\tilde{k}} \text{products} \qquad \text{(ii)}$$

in which the electron transfer step is assumed to be reversible and B decays by first order kinetics (rate constant, $\tilde{k}$). Specifically the calculation of current/voltage curves in this case allows us to deduce the variation of the halfwave potential with electrolyte flow rate and this behaviour is shown to be diagnostic

of the reaction type. The results are generalized in the form of a 'working curve' which relates the shift in halfwave potential, from the standard electrode potential E^0, to a normalized rate constant, so that the mechanism may be characterized experimentally and rate constant, $\tilde{k}$, deduced.

2. Theory

The convective-diffusion equations relevant to the EC mechanism in the WJE geometry, under steady-state conditions are:

$$v_r \frac{\partial[A]}{\partial r} + v_z \frac{\partial[A]}{\partial z} = D \frac{\partial^2[A]}{\partial z^2} \quad (1)$$

$$v_r \frac{\partial[B]}{\partial r} + v_z \frac{\partial[B]}{\partial z} = D \frac{\partial^2[B]}{\partial z^2} - \tilde{k}[B] \quad (2)$$

where the coordinates r and z are defined in Fig. 1 and D is the diffusion coefficient of A and B (assumed equal). The velocity of the solution is described by the two components, v_r for the radial direction, and v_z for the velocity in the direction normal to the electrode surface, for which, close to the electrode surface, the following approximations may be used [14]:

$$v_{r,\eta\to 0} = \frac{2}{9} \times \left(\frac{15M}{2\nu r^3}\right)^{\frac{1}{2}} \times \eta \quad (3)$$

$$v_{z,\eta\to 0} = \frac{7}{36} \times \left(\frac{40M\nu}{3r^5}\right)^{\frac{1}{2}} \times \eta^2 \quad (4)$$

where ν is the kinematic viscosity and η is a dimensionless parameter describing distance normal to the electrode given by,

$$\eta = \left(\frac{135M}{32\nu^3 r^5}\right)^{1/4} z, \quad (5)$$

and $M = k_c^4 V_f^3/2\pi^3 a^2$. In this V_f is the volume flow rate ($cm^3\ s^{-1}$), k_c is a constant determined by experiment to be close to 0.90 [14] and a is the diameter of the jet.

We assume that only A is present in bulk solution and normalize the concentrations relative to this bulk value, $[A]_0$, viz. $g(A) = [A]/[A]_0$ and $g(B) = [B]/[A]_0$. The boundary conditions are then:

(a) at the centre of the jet,

$$r = 0: \quad g(A) = 1, \quad g(B) = 0 \quad (6)$$

(b) in bulk solution,

$$z \longrightarrow \infty (\eta \sim 0.4): \quad g(A) = 1, \quad g(B) = 0 \quad (7)$$

(c) at the electrode surface,

$$z = 0: \quad g(A)/g(B) = \exp(\theta),$$
$$\partial g(A)/\partial z = -\partial g(B)/\partial z \quad (8)$$

where the normalized potential, $\theta = (F/RT)(E - E^0)$. Notice that, as discussed before, we restrict our calculations to the range $0 < \eta < 0.4$ which is the region in which the deviations from bulk concentrations are found [13].

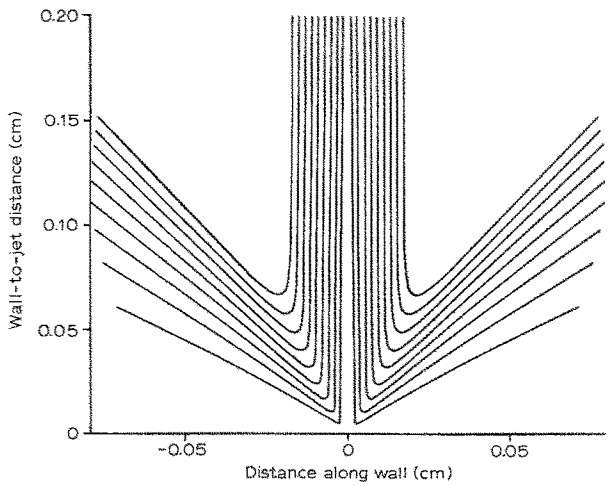

Fig. 1. Streamlines showing the flow pattern at the wall-jet electrode, calculated for an electrode with $a = 0.0345$ cm, $k_c = 0.9$ and a flow rate of 0.001 $cm^3\ s^{-1}$. The dimensions given on the diagram are in cm.

In order to solve the above equations we employ the 'expanding grid' BIFD method and proceed exactly as in reference [13] using the same notation as in that paper: in particular the subscripts on the normalized concentration $g_{j,k+1}$ denote distances in the radial ($j = 1, 2, \ldots, J$) and normal ($k = 1, 2, \ldots, K$) directions and $g_{j,k'}$ represents an interpolated concentration, deduced from $g_{j,k}$ used in the calculation of $g_{j,k+1}$ [13].

We thus arrive at two matrix equations, one for each of A and B such that,

$$\{\mathbf{d}\} = [\mathbf{T}].\{\mathbf{u}\} \quad (9)$$

where the matrix elements are as in reference [13] except:

(a) *Matrix elements for A*

$$d_j = g(A)_{j,k'} \quad j = 2, 3 \ldots, \overline{J-2} \quad (10)$$

$$d_{J-1} = g(A)_{J-1,k'} + \{\varepsilon_{J-1,k+1} - \lambda_{J-1,k+1}\} \quad (11)$$

$$d_1 = g(A)_{1,k'} + \frac{g(B)_{1,k+1}}{1 + \exp(-\theta)} \cdot \varepsilon_{1,k+1} \quad (12)$$

$$u_j = g(A)_{j,k+1} \quad j = 1, 2 \ldots \overline{J-1} \quad (13)$$

$$a_j = -\varepsilon_{j,k+1} \quad j = 2, 3 \ldots \overline{J-1} \quad (14)$$

$$b_j = (2\varepsilon_{j,k+1} - \lambda_{j,k+1} + 1) \quad j = 2, 3 \ldots \overline{J-1} \quad (15)$$

$$b_1 = \left[2 - \frac{1}{1 + \exp(-\theta)}\right] \varepsilon_{j,k+1} - \lambda_{j,k+1} + 1 \quad (16)$$

(b) *Matrix elements for B*

$$d_j = g(B)_{j,k'} \quad j = 2, 3 \ldots \overline{J-2} \quad (17)$$

$$d_1 = g(B)_{1,k'} + \frac{g(A)_{1,k+1}}{1 + \exp(\theta)} \cdot \varepsilon_{1,k+1} \quad (18)$$

$$u_j = g(B)_{j,k+1} \quad j = 1, 2 \ldots \overline{J-1} \quad (19)$$

$$a_j = -\varepsilon_{j,k+1} \quad j = 2, 3 \ldots \overline{J-1} \quad (20)$$

$$b_j = (2\varepsilon_{j,k+1} - \lambda_{j,k+1} + 1 + K_{j,k+1}) \quad j = 2, 3 \ldots \overline{J-1} \quad (21)$$

$$b_1 = \left[2 - \frac{1}{1 + \exp(\theta)}\right]\varepsilon_{j,k+1} - \lambda_{j,k+1} + 1 + K_{j,k+1} \quad (22)$$

where $\lambda_{j,k+1}$ and $\varepsilon_{j,k+1}$ have been defined in reference [13] and

$$K_{j,k+1} = \frac{\tilde{k}\Delta r}{v_r(j, k + 1)} \quad (23)$$

in which Δr is the size of the simulation grid in the radial direction. Notice that the matrix elements b_1 and d_1 arise from Equations 8 in finite difference form.

The matrix [**T**] is of tridiagonal form and this allows the use of the Thomas algorithm [17, 18] to calculate $\{\mathbf{u}\}_k$ from $\{\mathbf{d}\}_k$ provided that we specify a value for the electrode potential θ. The boundary condition $g_{j,0}$ ($j = 1, 2 \ldots J$) supplies the vector $\{\mathbf{d}\}_0$ from which $\{\mathbf{u}\}_0$ is calculated. But $\{\mathbf{d}\}_{k+1}$ is readily determined from $\{\mathbf{u}\}_k$ (Equations 10–13 or 17–19) so that $\{\mathbf{u}\}_1$ may then be calculated from $\{\mathbf{d}\}_1$, $\{\mathbf{u}\}_2$ from $\{\mathbf{d}\}_2$, and so on until $\{\mathbf{u}\}_k$ is obtained. In this way all the values $g_{j,k}$ ($j = 1, 2 \ldots J - 1$, $k = 1 \ldots K$) can be evaluated. However in comparison with the computations for simple electron transfer or for the ECE mechanism a complication presents itself: as can be seen from Equations 12 and 18 some matrix elements for A depend on $g(\mathrm{B})_{j,k+1}$ and some of those for B depend on $g(\mathrm{A})_{j,k+1}$. Thus in order to facilitate solution of the equations we employ an iterative method. Specifically an initial value of $g(\mathrm{B})_{j,k'}$ for $g(\mathrm{B})_{j,k+1}$ is assumed in order to permit the calculation of a value for $g(\mathrm{A})_{j,k+1}$. This value is then used to calculate a 'better' value of $g(\mathrm{B})_{j,k+1}$, and the process repeated until there is no significant change in either $g(\mathrm{A})_{j,k+1}$ or $g(\mathrm{B})_{j,k+1}$ on further iteration. The final values are then used to start the iterative calculation on the next line 'downstream', i.e. the concentrations $g_{j,k+2}$.

Finally the current flowing at the selected potential may be found using Equation 41 of [13]. By repeating the calculation for different values of θ the entire current/voltage curve can be deduced.

Computations were carried out using programs written in FORTRAN 77 on a VAX 11/785 mainframe computer, using NAG 11 library routines.

3. Results and discussion

Figure 2 shows typical current voltage curves generated as described above. These were calculated for three different rate constants: $\tilde{k} = 0$, 0.01 and 0.1 s^{-1} at a volume flow rate, $V_f = 0.001\,cm^3\,s^{-1}$, for a wall-jet electrode of radius, $R = 0.40\,cm$, with a jet diameter, $a = 0.0345\,cm$ and $k_c = 0.9$. The following parameters were also used: $v = 0.0089\,cm^2\,s^{-1}$; $D = 2 \times 10^{-6}\,cm^2\,s^{-1}$; $[A]_0 = 10^{-6}\,mol\,cm^{-3}$. In all calculations convergence was examined by varying the size of the computational grid used: for $\tilde{k} = 0$ values of $J = 200$ and $K = 5000$ were sufficient to give convergence to three significant figures in the computed current. These values increase with $\tilde{k}$: for $\tilde{k} = 0.1\,s^{-1}$ values of $J = 600$ and $K = 5000$ were needed. This is because the B concentration profile is increasingly constrained to within smaller distances of the electrode due to its shortened lifetime.

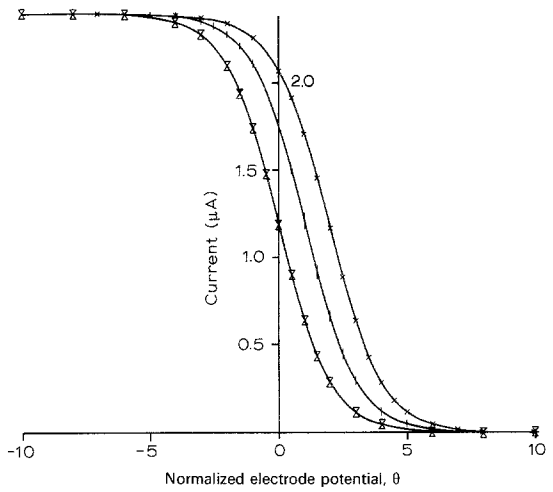

Fig. 2. Computed current/voltage curves for $k_{(ii)} = 0$ (x), 0.01 (1) and 0.1 (*) s^{-1} for a WJE of the dimensions specified in the text.

Examination of Fig. 2 shows that, as expected, the limiting current is independent of the value of $\tilde{k}$ and unchanged from that for a simple electron transfer process, but that as the rate constant increases the voltammetric reduction wave is shifted anodically as a result of the following chemical reaction. In all cases the computed transport limited current was in agreement with the analytical equation derived by Albery [14] for the one electron, no-kinetics case:

$$I_{LIM} = 1.59 k_c F D^{2/3} v^{-5/12} V_f^{3/4} a^{-1/2} R^{3/4} [A]_0 \quad (24)$$

where F is the Faraday constant. The shift in halfwave potential was found to be dependent on $\tilde{k}$, solution flow rate and electrode geometry. The relative contributions of each can be found by rewriting Equations 1–4. We define the new variables:

$$\xi = (r/R)^{9/8} \quad (25)$$

and

$$\chi = (9C/8D)^{1/3} (1/R)^{-3/8} (z/r^{7/8}) \quad (26)$$

where $C = ([5M]^3/216v^5)^{1/4}$. Equations 1 and 2 become:

$$\left(\frac{\partial^2[A]}{\partial\chi^2}\right) = \chi\left(\frac{\partial[A]}{\partial\xi}\right)_\chi \quad (27)$$

$$\left(\frac{\partial^2[B]}{\partial\chi^2}\right)_\xi = \chi\left(\frac{\partial[B]}{\partial\xi}\right)_\chi - K'\,\xi^{14/9}\,[B] \quad (28)$$

where,

$$K' = \tilde{k}.R^{5/2}\left(\frac{64}{81C^2D}\right)^{1/3} \quad (29)$$

It thus follows that each current/voltage curve is a function of the normalized rate constant K' only. The results of our calculations covering a wide range of rate constants, flow rates and electrode geometries can thus be presented in the form of a plot of the shift in halfwave potential, $\Delta\theta_{1/2} = (F/RT)(E_{1/2} - E^0)$,

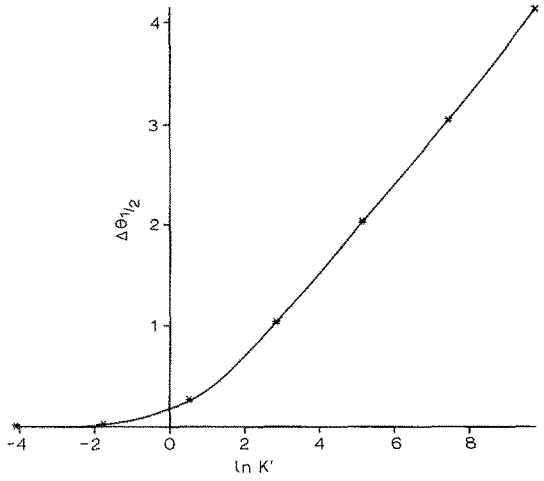

Fig. 3. A 'working curve' showing the shift in normalized halfwave potential, $\Delta\theta_{1/2} = (F/RT)(E_{1/2} - E^0)$, as a function of the normalized rate constant K' (Equation 29).

against K'. Such a 'working curve' is presented in Fig. 3 where ln K' is used as the abscissa. Data generated for parameters in the ranges R = 0.06–1.06 cm, $D = 2 \times 10^{-6}$–2×10^{-3} cm^2 s^{-1} and $\tilde{k}$ = 0.0–10.0 s^{-1} were all found to lie on the curve drawn. The curve provides the basis for the analysis of experimental data: observed shifts in halfwave potential are related to corresponding K' values should then have a flow rate dependence in agreement with Equation 29.

Finally we note that at high values of K' the slope of the curve in Fig. 3 tends towards 1/2. This behaviour can be rationalized [19] on the basis of the concept of a reaction layer much thinner than the diffusion layer. In this case the convective term $\chi(\partial[B]/\partial\xi)$ can be omitted from Equation 28. We thus find that,

$$[B] = [B]_* \exp(-K'^{1/2}\,\xi^{7/9}\,\chi) \qquad (30)$$

where $[B]_*$ is the surface concentration of B. Applying the boundary condition, Equation 8, to a point on the electrode at a radius ξ we have:

$$\{[A]_0 - [A]_*\}/\chi_d = (\partial[A]/\partial\chi)_{\xi=0} = -(\partial[B]/\partial\chi)_{\xi=0} = K'^{1/2}\,\xi^{7/9}\,[B]_* \qquad (31)$$

where $[A]_*$ is the surface concentration of A and $\chi_d(\xi)$ is the diffusion layer thickness at ξ. We thus find that,

$$-(\partial[B]/\partial\chi)_{\xi=0} = [A]_0/\{K'^{-1/2}\exp(\theta) + \xi^{7/9}\,\chi_d(\xi)\} \qquad (32)$$

so that the total electrode current,

$$I \propto \int_0^1 (\partial[B]/\partial\chi)_{\xi=0}\,d\chi = I(I_{LIM}, K'^{-1/2}\exp(\theta), \xi = 1) \qquad (33)$$

so that for $I = I_{LIM}/2$ we find that

$$\exp\{(F/RT)(E_{1/2} - E^0)\}/K'^{1/2} = g(\xi = 1) \qquad (34)$$

where g is an unspecified function. Hence

$$E_{1/2} - E^0 \propto (1/2)(RT/F)\ln K' \qquad (35)$$

as observed in Fig. 3.

In conclusion we have demonstrated that the 'expanding' grid BIFD method can be used to calculate current/voltage waveshapes at the WJE. The results in the case of the EC mechanism give rise to a 'universal' working curve which relates the shift in halfwave potential to a normalized rate constant and thus provides a means for the characterization of such reactions and for determining the rate constant $\tilde{k}$.

References

[1] M. B. Glauert, *J. Fluid Mech.* **1** (1956) 625.
[2] H. Gunasingham, K. P. Ang and C. C. Ngo, *Anal. Chem.* **57** (1985) 505.
[3] J. Wang and B. A. Freiha, *Anal. Chem.* **57** (1985) 1776.
[4] H. Gunasingham, K. P. Ang. C. C. Ngo and P. C. Thiak, *J. Electroanal. Chem* **198** (1986) 27.
[5] J. Wang, H. D. Dewald and B. Greene, *Anal. Chim. Acta* **146** (1983) 45.
[6] J. G. Douglas, *Anal. Chem.* **61** (1989) 922.
[7] H. Gunasingham, K. P. Ang and C. C. Ngo, *Analyst* **133** (1988) 1533.
[8] *Idem*, B. T. Tay and K. P. Ang, *Anal. Chem.* **56** (1984) 2422.
[9] *Idem*, *Anal. Chim. Acta* **159** (1984) 2422.
[10] C. M. A. Brett and A. M. C. F. Oliveira Brett, *J. Electroanal. Chem.* **262** (1989) 83.
[11] *Idem*, *Portugaliae Electrochimica Acta* **7** (1989) 21.
[12] *Idem*, *J. Electroanal. Chem.* **258** (1989) 345.
[13] R. G. Compton, C. R. Greaves and A. M. Waller, *J. Appl. Electrochem.* **20** (1990) 575.
[14] W. J. Alberg and C. M. A. Brett, *J. Electroanal. Chem.* **148** (1983) 201.
[15] J. Yamada amd H. Matsuda, *ibid.* **44** (1973) 189.
[16] R. G. Compton, C. R. Greaves and A. M. Waller, *J. Appl. Electrochem.* (in press).
[17] R. G. Compton, M. B. G. Pilkington and G. M. Stearn, *J. Chem. Soc. Faraday Trans. I* **84** (1988) 2155.
[18] L. Lapidus and G. Pinder, 'Numerical Solutions of Partial Differential Equations in Science and Engineering', John Wiley & Sons, New York (1982).
[19] B. A. Coles and R. G. Compton, *J. Electroanal. Chem.* **127** (1981) 37.